

Importance of the heavy-quarks longitudinal structure function measurements at future circular collider energies

G.R.Boroun*

Physics Department, Razi University, Kermanshah 67149, Iran
(Dated: February 28, 2025)

In this article, we consider the ratio of structure functions for heavy quark pair production at low values of x . The importance of this ratio for charm and beauty pair production is examined according to the Hadron Electron Ring Accelerator (HERA) data. The behavior of these ratios considers due to the hard-pomeron behavior of the gluon distribution function. The results are in good agreement with respect to the HERA data. Expanding this data to the range of new energies underscore the importance of these measurements for heavy quarks. The ratio of charm and beauty structure functions at the proposed Large Hadron electron Collider (LHeC) is considered as a function of invariant center-of-mass energy. For top pair production this ratio is extracted with known kinematics of the LHeC and Future Circular Collider electron-hadron (FCC-eh) colliders. Comparison of the results obtained for the ratio of top structure functions in LHeC and FCC-eh are proportional to the specified inelasticity y range.

1. Introduction

The latest data collected in HERA for heavy quarks show that the cross sections for charm and beauty production can be considered in a wide range of x and Q^2 values from the H1 and ZEUS detectors [1-4]. Also a combination method at HERA used for the cross section data with respect to the correlations of the statistical and systematic uncertainties. In neutral current (NC) deep inelastic electron-proton scattering (DIS) at HERA, heavy-quarks production is the most important quantum chromodynamics (QCD) tests. The dominant process in the production of heavy quarks is Boson-gluon-fusion (BGF). The production of heavy quarks at HERA depends on the mass of these quarks and thus the calculations of cross sections depend on a wide range of perturbative scales μ^2 . The massive fixed-flavour-number scheme (FFNS) [5] and the variable-flavour-number scheme (VFNS) [6] are different approaches for considering heavy quarks. FFNS can be used on the threshold of $\mu^2 \approx m^2$ and for $\mu^2 \gg m^2$ VFNS is used where the treatment of resummation of collinear logarithms $\ln(\mu^2/m^2)$ is achieved. In Ref.[7] a general-mass variable-flavour-number scheme (GM-VFNS) for calculation of the contributions of heavy quarks introduced.

In the process $\gamma^* g \rightarrow Q\bar{Q}$, where Q is heavy quark, heavy-quark production is sensitive to the gluon distribution and gluon momentum transfer in the proton. In accordance with the heavy quarks mass, the gluon momentum is arranged such that $x_g^t > x_g^b > x_g^c$. HERA dataset, for production charm and beauty in DIS, covers the kinematic range of photon virtuality $2.5 \leq Q^2 \leq 2000 \text{ GeV}^2$ and Bjorken scaling variable $3.10^{-5} \leq x \leq 5.10^{-2}$ [1-4]. The ep center-of-mass energies with data taken with the H1 and ZEUS detectors are corresponding to $\sqrt{s} = 319 \text{ GeV}$ [1] and $\sqrt{s} = 318 \text{ GeV}$ [2] respectively. Future circular electron proton colliders are the ideal environment to increase center-of-mass energy [8-10]. At LHeC, the electron-proton center of mass energy reach to $\sqrt{s} \simeq 1.3 \text{ TeV}$. The x, Q^2 values of simulated heavy quark density data used in LHeC studies reach to $x \leq 10^{-5}$ and $Q^2 \geq 10^4 \text{ GeV}^2$ [9]. Also the heavy quark densities will be checked at FCC-eh programme which the center-of-mass energy reaches $\simeq 3.5 \text{ TeV}$ [10].

The heavy-quark structure functions obtained in DIS at HERA, from the measurement of the inclusive heavy quark cross sections, are an important test of the QCD. These structure functions are obtained after applying small corrections for the heavy-quark longitudinal structure functions [1-4]. The heavy-quark cross section defined in terms of the heavy-quark structure functions as

$$\frac{d^2\sigma^{Q\bar{Q}}}{dx dQ^2} = \frac{2\pi\alpha^2(Q^2)}{xQ^4} \{[1 + (1-y)^2]F_2^{Q\bar{Q}}(x, Q^2) - y^2 F_L^{Q\bar{Q}}(x, Q^2)\}, \quad (1)$$

*Electronic address: grboroun@gmail.com; boroun@razi.ac.ir

where y is the inelasticity. The reduced cross section defined as follows

$$\begin{aligned}\sigma_{\text{red}}^{\mathcal{Q}\overline{\mathcal{Q}}} &= \frac{d^2\sigma^{\mathcal{Q}\overline{\mathcal{Q}}}}{dx dQ^2} \cdot \frac{xQ^4}{2\pi\alpha^2(Q^2)(1+(1-y)^2)} \\ &= F_2^{\mathcal{Q}\overline{\mathcal{Q}}}(x, Q^2) - f(y)F_L^{\mathcal{Q}\overline{\mathcal{Q}}}(x, Q^2),\end{aligned}\quad (2)$$

where $f(y) = \frac{y^2}{1+(1-y)^2}$. In HERA kinematic range the contribution $F_L^{\mathcal{Q}\overline{\mathcal{Q}}}$ is small. Therefore the heavy-quark structure function $F_2^{\mathcal{Q}\overline{\mathcal{Q}}}$ is obtained from the measured heavy-quark cross sections. The measurements of $\sigma_{\text{red}}^{\mathcal{Q}\overline{\mathcal{Q}}}$, based on data from HERA I and HERA II, are shown as a function of x for fixed values of Q^2 in Refs.[1-4]. The measured values of heavy-quark structure functions $F_2^{\mathcal{Q}\overline{\mathcal{Q}}}$ were obtained using

$$F_2^{\mathcal{Q}\overline{\mathcal{Q}}}(x, Q^2) = \frac{d^2\sigma_{\mathcal{Q}}^{\text{jet}}/dx dQ^2}{d^2\sigma_{\mathcal{Q}}^{\text{had,NLO}}/dx dQ^2} F_2^{\mathcal{Q}\overline{\mathcal{Q}},\text{NLO}}(x, Q^2) \quad (3)$$

The differential cross section for jet production method is defined in literature and also NLO QCD predictions were obtained from the FFNS using HVQDIS program [11]. This method is also used for the heavy-quark longitudinal structure function to the cross section. Heavy-quark cross sections were determined and extracted in analogy to $F_2^{\mathcal{Q}\overline{\mathcal{Q}}}$. In this way no assumption on $F_L^{\mathcal{Q}\overline{\mathcal{Q}}}$ was required. Indeed

$$\sigma_{\text{red}}^{\mathcal{Q}\overline{\mathcal{Q}}} = F_2^{\mathcal{Q}\overline{\mathcal{Q}}}(x, Q^2)[1 - f(y)F_L^{\mathcal{Q}\overline{\mathcal{Q}}}(x, Q^2)/F_2^{\mathcal{Q}\overline{\mathcal{Q}}}(x, Q^2)] \quad (4)$$

Future circular colliders will extend the ratio $F_L^{\mathcal{Q}\overline{\mathcal{Q}}}/F_2^{\mathcal{Q}\overline{\mathcal{Q}}}$ into a region of much smaller x and higher Q^2 . Indeed the LHeC is the ideal place to resolve this ratio [9]. Overview of the kinematic plane of the LHeC pseudo-data [12,13] is illustrated in Table I for the x, Q^2 values of simulated heavy quark density data [9,14]. These data provide additional constraints on the gluon.

The paper is organized as follows. In sect.2, we give a summary about the ratio of heavy-quark structure functions. Then we introduce a method to calculate the ratio $F_L^{\mathcal{Q}\overline{\mathcal{Q}}}/F_2^{\mathcal{Q}\overline{\mathcal{Q}}}$ applying the gluon exponent. After reviewing the essential features of the charm and beauty structure functions at HERA in section 3, we will study the heavy-quark structure functions at the LHeC and FCC-eh kinematics in this section. Section 4 contain the results and discussions. Our summary and conclusion are given in section 5.

2. A Short Theoretical Input

The dynamics of flavor-singlet quark and gluon distribution functions, q^s and g , are defined by

$$\begin{aligned}q^s(x, n_f, \mu^2) &= \sum_{l=1}^{n_f} [f_l(x, n_f, \mu^2) + \overline{f}_l(x, n_f, \mu^2)], \\ g(x, n_f, \mu^2) &= f_g(x, n_f, \mu^2),\end{aligned}\quad (5)$$

where n_f is number of active quark flavor. The heavy-quark structure functions derived using the zero-mass VFN scheme (ZMVFN) as

$$F_{k,Q}^{\text{ZMVFN}} = \sum_{j=0}^{\infty} a_s^j(n_f+1) \sum_{i=q,g,Q} C_{k,i}^{(j)}(n_f+1) \otimes f_i(n_f+1) \quad (6)$$

where C 's are the Wilson coefficients at the j -th order and $k=2$ and L . Here $a_s = \frac{\alpha_s}{4\pi}$ is the QCD running coupling. Eq.(6), at asymptotically large momentum transfer $Q^2 \gg m_Q^2$, is valid. For $Q^2 \simeq m_Q^2$ VFNS is valid which it includes a combination of the ZMVFN with FFNS. In this case the heavy-quark structure functions are

$$F_{k,Q}^{\text{FFNS}} = \sum_{j=0}^{\infty} a_s^j(n_f) \sum_{i=q,g} H_{k,i}^{(j)}(n_f) \otimes f_i(n_f), \quad (7)$$

where H 's are the Wilson coefficients for the DIS heavy-quark production [15]. In the following, we suppress the dependence on the active flavor n_f . In GM-VFNS one should take into account quark mass as the rescaling variable χ is defined into the Bjorken variable x by the following form [16]

$$\chi = x(1 + \frac{4m_Q^2}{Q^2}), \quad (8)$$

where the rescaling variable, at high Q^2 values ($m_Q^2/Q^2 \ll 1$), reduces to x , $\chi \rightarrow x$. Here m_Q is the heavy quark mass. Within this scheme heavy quark densities arise via the $g \rightarrow Q\bar{Q}$ evolution. In the small- x range the heavy quark contributions are given by these forms

$$\begin{aligned} F_2^{Q\bar{Q}}(x, Q^2) &= C_{2,g}^{Q\bar{Q}}(x, \xi) \otimes G(x, \mu^2), \\ F_L^{Q\bar{Q}}(x, Q^2) &= C_{L,g}^{Q\bar{Q}}(x, \xi) \otimes G(x, \mu^2). \end{aligned} \quad (9)$$

where $\xi = \frac{m_Q^2}{Q^2}$. The coefficient functions up to NLO analysis, $C_{2,g}$ and $C_{L,g}$, demonstrated in Refs.[5,15,17]. \otimes note the convolution between two functions of x as, $[f \otimes g](x) = \int_x^1 (dy/y) f(y) g(x/y) = \int_x^1 (dz/z) f(x/z) g(z)$. Here $G(x, \mu^2) (= xg(x, \mu^2))$ is the gluon momentum distribution and the default renormalisation scale μ_r and factorization scale μ_f are set to $\mu \equiv \mu_r = \mu_f = \sqrt{Q^2 + 4m_Q^2}$. Within the pQCD, and up to the NLO corrections, the coefficient functions $C_{2,g}$ and $C_{L,g}$ read as

$$C_{k,g}(z, \xi) = C_{k,g}^0(z, \xi) + a_s(\mu^2) C_{k,g}^1(z, \xi). \quad (10)$$

The behavior of the heavy-quark structure function is governed entirely by the hard pomeron exchange in accordance with the Regge theory. The heavy quark cross section depends strongly on the gluon distribution which the density of gluons enter at

$$x_g^Q = \frac{Q^2 + M_t^2}{W^2 + Q^2} = x_{bj}(1 + \frac{M_t^2}{Q^2}), \quad (11)$$

where M_t is the transverse mass of the produced heavy quark pair $Q\bar{Q}$ [18]. The standard parameterization of the gluon distribution function at low x observed by the following form

$$G(x, Q^2)_{x \rightarrow 0} = f_g(Q^2) x^{-\lambda_g(Q^2)}. \quad (12)$$

Over a wide range of Q^2 , the gluon density behaves as a fixed power of x as the quantity λ_g is the hard-pomeron intercept minus one¹. Eq.(12) granted originates of heavy quarks from gluons in the proton. Indeed the heavy-quark structure functions can be described by a fixed power of x behavior [19,20] as

$$F_2^{c(b)} = f_Q(Q^2) x^{-\lambda_{eff}}. \quad (13)$$

The gluon exponent at low values of x is described by the hard-pomeron as the fixed coupling LLx BFKL solution gives the value $\lambda_g \simeq -0.5$. Although dependence on Q^2 is expressed in effective exponent defined in Ref.[21]. In literatures, fit to experimental data suggests that hard pomeron dominate the behavior of the heavy quark structure function. It is suggested that this behavior can be shown in the form of Eq.(13), which we assume that $\lambda_{eff}^c \simeq \lambda_{eff}^b$. Because the heavy quark behavior at low x is determined by the gluon behavior, so $\lambda_{eff}^c \simeq \lambda_{eff}^b = \lambda_g$.

Within the dipole formulation of the γ^*p scattering [22], the gluon density is modelled as $xg(x, \mu^2) = \frac{3}{4\pi^2\alpha_s} \frac{\sigma_0}{R_0^2(x)}$, where $R_0(x)$ is the saturation scale. This function decreases when $x \rightarrow 0$ as $R_0^2(x) = \frac{1}{\text{GeV}^2} (\frac{x}{x_0})^{\lambda_g}$. The parameters of the model (i.e., σ_0 and x_0) are defined in Ref.[22]. In color dipole model (CDM) the saturation exponent λ_g is defined from a fit to low x data as $\lambda_g \simeq 0.3$. In this analysis, we will try to select the gluon exponent value corresponding to the average of the hard pomeron and color dipole model, where $0.3 \leq \lambda_g \leq 0.5$. Here the lower limit corresponds to the

¹ Authors in Refs.[19] obtained a good numerical fit to the output of the DGLAP evolution for the gluon distribution at low x by the following form $G(x, Q^2) = f_g(Q^2) x^{-\epsilon_0}$ where ϵ_0 is hard pomeron exchange. Over a wide range of Q^2 values, the charm structure function behaves as a fixed power of x as $F_2^c(x, Q^2) = f_c(Q^2) x^{-\epsilon_0}$.

saturation exponent and the upper limit corresponds to the hard pomeron exponent.

In recent years [23,24], the phenomenological various successful methods have examined charm and beauty structure functions. This importance, along with the t-quark density, can be explored at future circular collider energies. One of the important top quark production modes is $t\bar{t}$ photoproduction [26,26,27]. The total cross section prediction at LHeC is 0.05 pb [28]. These studies lead us to new physics in the future.

3. Method

Based on the hard-pomeron behavior of the distribution functions, the ratio of heavy-quark structure functions is formulated based on the coefficient functions and gluon exponent. After doing the integration over z , the ratio F_L/F_2 for heavy quarks can be rewritten in a convolution form as the ratio $F_L^{\mathcal{Q}\overline{\mathcal{Q}}}/F_2^{\mathcal{Q}\overline{\mathcal{Q}}}$ is defined by

$$\frac{F_L^{\mathcal{Q}\overline{\mathcal{Q}}}}{F_2^{\mathcal{Q}\overline{\mathcal{Q}}}} = \frac{C_{L,g}^{\mathcal{Q}\overline{\mathcal{Q}}}(x, \xi) \odot x^{\lambda_g}}{C_{2,g}^{\mathcal{Q}\overline{\mathcal{Q}}}(x, \xi) \odot x^{\lambda_g}}, \quad (14)$$

where $[f \odot g](x) = \int_x^1 (dy/y) f(y) g(y)$. In the analytical form, power-like behavior of the heavy-quark structure functions is generically written as follows

$$\begin{aligned} \frac{\partial}{\partial \ln \frac{1}{x}} \ln \frac{F_L^{\mathcal{Q}\overline{\mathcal{Q}}}(x, Q^2)}{F_2^{\mathcal{Q}\overline{\mathcal{Q}}}(x, Q^2)} &= \lambda_L^{\mathcal{Q}\overline{\mathcal{Q}}} - \lambda_2^{\mathcal{Q}\overline{\mathcal{Q}}} \\ &= \frac{\partial}{\partial \ln \frac{1}{x}} \ln \frac{C_{L,g}^{\mathcal{Q}\overline{\mathcal{Q}}}(x, \xi) \odot x^{\lambda_g}}{C_{2,g}^{\mathcal{Q}\overline{\mathcal{Q}}}(x, \xi) \odot x^{\lambda_g}}. \end{aligned} \quad (15)$$

The exponents λ_L and λ_2 for heavy-quark production are defined by the derivatives of the heavy-quark structure functions by the following forms

$$\begin{aligned} \lambda_L^{\mathcal{Q}\overline{\mathcal{Q}}} &= \partial \ln F_L^{\mathcal{Q}\overline{\mathcal{Q}}}(x, Q^2) / \partial \ln(1/x), \\ \lambda_2^{\mathcal{Q}\overline{\mathcal{Q}}} &= \partial \ln F_2^{\mathcal{Q}\overline{\mathcal{Q}}}(x, Q^2) / \partial \ln(1/x). \end{aligned} \quad (16)$$

The importance of the relationship between $\sigma_{\text{red}}^{\mathcal{Q}\overline{\mathcal{Q}}}$ and $F_2^{\mathcal{Q}\overline{\mathcal{Q}}}(x, Q^2)$ in Eq.(4) depends on the functions of $f(y)$ and the ratio $F_L^{\mathcal{Q}\overline{\mathcal{Q}}}/F_2^{\mathcal{Q}\overline{\mathcal{Q}}}$. In the high inelasticity which $f(y) \rightarrow 1$, the importance of the longitudinal structure function in the production of heavy pair quarks is revealed in the LHeC and FCC-eh. In comparisons with the latest data collected in HERA [3], we can see an increase in values of Q^2 and a decrease in values of x in new energies.

HERA data are expressed in terms of two variables, x and Q^2 . At low x we define a new variable that $Q^2/x \simeq W^2$. W^2 refers to the photon-proton center-of-mass energy. Indeed the heavy-quark structure functions are given by the single variable W^2 as

$$\begin{aligned} F_L^{\mathcal{Q}\overline{\mathcal{Q}}}(x, Q^2) &= F_L^{\mathcal{Q}\overline{\mathcal{Q}}}(W^2 = \frac{x}{Q^2}, Q^2), \\ F_2^{\mathcal{Q}\overline{\mathcal{Q}}}(x, Q^2) &= F_2^{\mathcal{Q}\overline{\mathcal{Q}}}(W^2 = \frac{x}{Q^2}, Q^2). \end{aligned} \quad (17)$$

According to power-like behavior, the heavy quark structure functions can be stated as

$$\begin{aligned} F_L^{\mathcal{Q}\overline{\mathcal{Q}}}(W^2) &\sim (W^2)^{\lambda_L}, \\ F_2^{\mathcal{Q}\overline{\mathcal{Q}}}(W^2) &\sim (W^2)^{\lambda_2}. \end{aligned} \quad (18)$$

The exponents now are defined by the following forms

$$\begin{aligned} \lambda_L^{\mathcal{Q}\overline{\mathcal{Q}}} &= \frac{\partial \ln F_L^{\mathcal{Q}\overline{\mathcal{Q}}}(W^2)}{\partial \ln W^2}, \\ \lambda_2^{\mathcal{Q}\overline{\mathcal{Q}}} &= \frac{\partial \ln F_2^{\mathcal{Q}\overline{\mathcal{Q}}}(W^2)}{\partial \ln W^2}. \end{aligned} \quad (19)$$

$$\begin{aligned}
\Rightarrow \Delta\lambda_{L2}^{Q\overline{Q}} &= \lambda_L^{Q\overline{Q}} - \lambda_2^{Q\overline{Q}} \\
&= \frac{\partial}{\partial \ln W^2} \ln \frac{F_L^{Q\overline{Q}}(W^2)}{F_2^{Q\overline{Q}}(W^2)}.
\end{aligned} \tag{20}$$

4. Results

4.1 : Charm and Beauty

In Refs.[1] and [2], the reduced cross sections and structure functions of the charm and beauty quarks in center-of-mass energies $\sqrt{s} = 319$ GeV and $\sqrt{s} = 318$ GeV can be observed respectively. The mass of the charm and beauty quarks set to $m_c = 1.5$ GeV and $m_b = 4.75$ GeV respectively. The extracted values of $\frac{F_L^{c\overline{c}}}{F_2^{c\overline{c}}}$ and $\frac{F_L^{b\overline{b}}}{F_2^{b\overline{b}}}$ into HERA data in Refs.[1] and [2] are given in figures 1 and 2 respectively. In these figures the ratio of structure functions for the charm and beauty quarks is plotted into a wide range of the invariant of mass W^2 . Calculations allowing the invariant mass W^2 to vary in the interval ($5000 < W^2 < 60000$ GeV²) when x and Q^2 varies according to HERA data. We observed that these ratio of structure functions are statistically very scattered. However, according to the Eqs.(19), the linear fit of these HERA data indicates the difference between intercepts for charm and beauty quarks production. The results of this linear fit are given in Table 2. Our belief is that the behavior of $\lambda_2^{Q\overline{Q}}$ corresponds to hard pomeron behavior. Based on this, $\lambda_L^{Q\overline{Q}}$ intercept can be determined based on HERA data. Nevertheless the data have the striking property that the ratio of structure functions behave by the following form

$$\frac{F_L^{Q\overline{Q}}(W^2)}{F_2^{Q\overline{Q}}(W^2)} \cdot \frac{f_2^{Q\overline{Q}}}{f_L^{Q\overline{Q}}} = (W^2)^{\Delta\lambda_{L2}^{Q\overline{Q}}}, \tag{21}$$

where $F_{2,L}^{Q\overline{Q}}(W^2) \simeq f_{2,L}^{Q\overline{Q}}(W^2)^{\lambda_{2,L}}$. Figure 3 shows this ratio (i.e., Eq.(21)) according to Table II and shows that the importance of measuring the longitudinal structure function for beauty quark is not less than charm quark. In this figure, $\Delta\lambda = \lambda_L - \lambda_2$ is obtained from a linear fit to the heavy quark structure functions into the invariant center-of-mass energy. Because the heavy-quark longitudinal structure function data scatter is high for H1 and ZEUS (according to Figs.1 and 2), therefore the linear fit of the data shows a noticeable difference in this figure. However, these fits can give comparable results below. According to Eq.(14), our results for the ratio $F_L^{Q\overline{Q}}/F_2^{Q\overline{Q}}$ are described in Fig.4 for charm and beauty quarks in a wide range of the invariant mass W^2 . The mass of charm and beauty quarks are defined according to Table III. In this figure, our results at $Q^2 = 60$ and 80 GeV² are compared with HERA data in Refs.[1,2]. These results are comparable with HERA data. As we see in this figure (i.e., Fig.4), the value of this ratio is almost constant in a wide range of the invariant mass. This ratio for the charm quark at both Q^2 values is almost 0.21 and for the beauty quark is almost 0.13 – 0.15. This conclusion for charm quark is close to the results Refs.[17,23,29]. In Fig.5 we present the ratio $F_L^{Q\overline{Q}}/F_2^{Q\overline{Q}}$ for charm and beauty quarks as a function of Q^2 at $W = 200$ GeV. We can see that obtained results are in agreement with others. The maximum value for charm and beauty ratios is the same and is equal to $\simeq 0.21$ in a wide range of Q^2 values. This maximum value shifts to larger Q^2 values for beauty quark. Indeed it shifts from $Q^2 \simeq 60$ GeV² for charm to $Q^2 \simeq 800$ GeV² for beauty quark. In these calculations, the errors are due to calculation errors related to the charm and beauty quarks mass and the gluon intercept. Indeed, the average between the hard-pomeron and color dipole models for the gluon exponent is assumed that $\lambda_g = 0.4 \pm 0.1$. In this figure we also compared our results for the ratio of structure functions for charm and beauty with HERA data [1,2]. Although errors related to the experimental data are not available, but the comparison of these results with HERA data are very good. It should be noted that the data collected from HERA is related to $175 < W < 225$ GeV, and this is the reason for the error between our results (at $W = 200$ GeV) and HERA data.

Now we focus attention on the energy shift from HERA to LHeC. LHeC data will also allow us to increase our knowledge of heavy flavour structure functions [30]. Due to the increase in center-of-mass energy in new colliders, the LHeC provides data on charm and beauty structure functions extending over nearly 5 and 6 orders of magnitude in x and Q^2 respectively [9]. According to the predicted energy range for LHeC, the center-of-mass energy changes as follows, $10^2 \leq W^2 \leq 10^6$ GeV². In Fig.6, phenomenological predictions of the charm and beauty structure functions are determined in center-of-mass energy $\sqrt{s} = 1.3$ TeV. We can see that as the energy increases, the maximum values for these ratios are still the same as $\simeq 0.21$. But the amount of Q^2 values increases slightly, as the maximum ratio value $F_L^{c\overline{c}}/F_2^{c\overline{c}}$ is in the order $\mathcal{O}(100 \text{ GeV}^2)$ and the maximum ratio value $F_L^{b\overline{b}}/F_2^{b\overline{b}}$ is in the order $\mathcal{O}(1000 \text{ GeV}^2)$. In

this figure (i.e., Fig.6), we show the Q^2 dependents of the heavy-quarks structure functions evaluated at NLO analysis.

4.2 : Top

Top-quark pairs can be produced the LHeC and FCC-eh from $\gamma^*p \rightarrow t\bar{t}$ reactions. Deep inelastic scattering measurements at LHeC and FCC-eh will allow the determination of the top distribution function. The production of top quarks in ep collisions at LHeC and FCC-eh can be provided a stringent test of new physics at ultra-high energy (UHE), which the center-of-mass energies are 1.3 TeV and 3.5 TeV respectively. One of the QCD corrections in top quarks production is the QCD coupling $\alpha_s(\mu^2)$ ($\mu^2 \propto \beta^2 \hat{s}$ where β is the $Q\bar{Q}$ relative velocity and $\hat{s} = 4m_t^2$) [30]. The running coupling constant at LHeC is the H1 result at NNLO analysis with 0.2% uncertainty from the LHeC and 0.1% uncertainty when combined with HERA data [8,9,10,31]. Here we used the active flavor number $n_f = 6$ in the running of α_s [9,10]. Because the top threshold is high enough, therefore the range of inelasticity changes is very important in determining the ratio $F_L^{t\bar{t}}/F_2^{t\bar{t}}$. For $Q^2 = 40000 - 50000 \text{ GeV}^2$ where $Q^2 > m_t^2$ ($m_t = 172 \pm 0.5 \text{ GeV}$), the area available in the further colliders covers the inelasticity from $0.300 < y < 0.800$ and $0.080 < y < 0.850$ at LHeC and FCC-eh respectively. The Wilson coefficient functions are experiencing a slow rescaling by replacing $z \rightarrow \chi$. This changes the integration range of z in the convolutions to $x(1 + \frac{4m_t^2}{Q^2}) \leq z \leq 1$ with the Bjorken variable x [15]. In the following we will discuss the ratio $F_L^{t\bar{t}}/F_2^{t\bar{t}}$ in the $t\bar{t}$ production at the LHeC and FCC-eh. In Fig.7 we present this ratio for $Q^2 = 40000$ and 50000 GeV^2 as a function of W^2 . Because $0 < y \leq 1$ then the range of x changes is very limited. Notice that the large inelasticity is only for scattered electron energies much smaller than the electron beam energy (i.e., $E'_e \ll E_e$ and $y = 1 - E'_e/E_e$). In this region which E'_e is small, the electromagnetic and hadronic backgrounds are important [9]. The maximum value for the ratio $F_L^{t\bar{t}}/F_2^{t\bar{t}}$ with respect to the inelasticities (i.e., $0.300 < y < 0.800$ and $0.080 < y < 0.850$ at LHeC and FCC-eh, respectively) is almost $\simeq 0.1$. Of course, this value for the ratio $F_L^{t\bar{t}}/F_2^{t\bar{t}}$ also increases to $\simeq 0.21$, when both Q^2 and x values increase. In this regard, the Q^2 value must be of order $\mathcal{O}(100000 \text{ GeV}^2)$ at LHeC and of order $\mathcal{O}(1000000 \text{ GeV}^2)$ at FCC-eh and the x value of order $\mathcal{O}(0.1)$. All these predictions can be seen in Fig.8. In this figure, the ratio of structure functions results for charm, beauty and top pair production are visible in the range of energies available for future accelerators. However, this range of x and Q^2 will be seen in future accelerations.

For the calculations presented, we considered the mass error and the gluon exponent error. In all figures, bandwidth errors are included. In Fig.9, we considered the effect of the renormalization/factorization scale uncertainty in the ratio F_L/F_2 for charm and beauty due to the LHeC center of mass energy. The left and right panels of Fig.9 show the ratio F_L/F_2 for charm and beauty as a function of Q^2 for $x = 0.001$ respectively. Our NLO results for $\mu_{c(b)} = 2m_{c(b)}$ and $\mu_{c(b)} = \sqrt{4m_{c(b)}^2 + Q^2}$ are presented in this figure, where they are compared with the quantities represented in Refs.[17](A. Y. Illarionov, B. A. Kniehl and A. V. Kotikov, Phys.Lett. B **663**, 66 (2008)) and [23](N.Ya.Ivanov, and B.A.Kniehl, Eur.Phys.J.C**59**, 647(2009)). In both references, the ratios are independent of the choice of the gluon distribution. These approaches based on perturbative QCD and k_T factorization gives similar predictions for the ratio of the heavy-quark structure functions. One of them (N.Ya.Ivanov, and B.A.Kniehl, Eur.Phys.J.C**59**, 647(2009)) provide analytical result for the ratio of structure functions for arbitrary values of the parameter λ_g in terms of the Gauss hypergeometric function. Those consider compact formulae for the ratio in two particular cases $\lambda_g = 0$ and $\lambda_g = 0.5$. The simplest case leads to a non-singular behavior at small x for the structure functions and another one (i.e., $\lambda_g = 0.5$) originates from the BFKL resummation of the leading powers of $\ln(1/x)$. In another reference, authors provide compact formulas for the ratio of structure functions with respect to the Mellin transform. In the following for low and moderate Q^2 one should take into account quark mass. So we replace $x \rightarrow (1 + \frac{4m_c^2}{Q^2})x$ in the formula for the ratio of heavy-quark structure functions. The behavior of the ratios are much less sensitive to the choice of scale μ at low and moderate values of Q^2 , as seen by comparing the corresponding curves in the two figures. For $Q^2 \gg 4m_{c(b)}^2$ the NLO predictions exhibit an appreciable scale dependence. One can see that all the considered NLO predictions agree with the literature results with a good accuracy.

5. Summary and Conclusion

We presented the ratio $F_L^{Q\bar{Q}}/F_2^{Q\bar{Q}}$ for charm and beauty pair production with respect to HERA data. The behavior of these ratios are in good agreement in comparison with experimental data in a wide range of W^2 values. Indeed a power-law behavior for the ratio of structure functions for heavy quark pair production is predicted.

Results as a function of Q^2 for an invariant constant value are in agreement with those extracted in literature in the framework of perturbative QCD. Then we have studied the production of heavy-pair quarks in new electron proton collisions (i.e., LHeC and FCC-eh). The ratio of charm and beauty structure functions are studied in center of mass energy $\sqrt{s} = 1.3$ TeV which proposed at LHeC collider. For the top quark pair production, which will be one kind of important production channel at LHeC and FCC-eh, the ratio of structure functions determined and compared together with respect to the center-of-mass energies in new colliders. The results of numerical calculations for heavy quarks in LHeC and FCC-eh are available with respect to the inelasticity defined in accordance with the center of mass energies. These results highlight the importance of measuring the longitudinal structure function in the production of heavy quarks in the future with respect to the energies available in the new accelerators.

ACKNOWLEDGMENTS

The authors are thankful to the Razi University for financial support of this project. The authors are especially grateful to Max Klein for carefully reading the manuscript and fruitful discussions. G.R.Boroun thanks H.Khanpour for interesting and useful discursions.

TABLE I: Illustration of the kinematic covrage of simulated heavy quark structure functions used in LHeC studies. The number of pseudo-data points, N_{dat} and the integrated luminosity, $\mathcal{L}_{int}[\text{ab}^{-1}]$, are shown in this table [9,14].

Observable	E_e	E_p	Kinematics	N_{dat}	$\mathcal{L}_{int}[\text{ab}^{-1}]$
$F_2^{c,NC}(e^-p)$	60 GeV	7 TeV	$7 \times 10^{-6} \leq x \leq 0.3, 4 \leq Q^2 \leq 2 \times 10^5 \text{ GeV}^2$	111	1.0
$F_2^{b,NC}(e^-p)$	60 GeV	7 TeV	$3 \times 10^{-5} \leq x \leq 0.3, 32 \leq Q^2 \leq 2 \times 10^5 \text{ GeV}^2$	77	1.0

TABLE II: $\Delta\lambda_{L2}^{\mathcal{Q}\overline{\mathcal{Q}}} = \lambda_L^{\mathcal{Q}\overline{\mathcal{Q}}} - \lambda_2^{\mathcal{Q}\overline{\mathcal{Q}}}$ determined for heavy-quark pair production (HQPP) according to HERA collected data in Refs.[1,2].

$HQPP$	$\Delta\lambda_{L2}^{\mathcal{Q}\overline{\mathcal{Q}}}$	Coll.Data
$c\overline{c}$	~ -0.68	Ref.[1]
$c\overline{c}$	~ -0.77	Ref.[2]
$b\overline{b}$	~ -0.24	Ref.[1]
$b\overline{b}$	~ -0.41	Ref.[2]

TABLE III: Heavy quarks mass with respect to the statistical and systematic uncertainties [3].

Quark	Mass	exp/fit	Model	Parameterization
c	1.290 GeV	$+0.046$ -0.041	$+0.062$ -0.014	$+0.003$ -0.031
b	4.049 GeV	$+0.104$ -0.109	$+0.090$ -0.032	$+0.001$ -0.031

REFERENCES

1. F.D.Aaron et al., [H1 Collaboration], *Eur.Phys.J.C***65**, 89 (2010).
2. H.Abramowicz et al., [ZEUS Collaboration], *JHEP***09**, 127 (2014).
3. H.Abramowicz et al., [H1 and ZEUS Collaboration], *Eur.Phys.J.C***78**, 473(2018).
4. H.Abramowicz et al., [H1 and ZEUS Collaboration], DESY-12-172, arXiv:1211.1182v2 [hep-ex](2012); H.Abramowicz et al., [ZEUS Collaboration], *Eur.Phys.J.C***69**, 347 (2010).
5. E. Laenen et al., *Phys. Lett. B***291**, 325 (1992); E. Laenen et al., *Nucl. Phys. B***392**, 162 (1993); S. Riemersma, J. Smith, W.L. van Neerven, *Phys. Lett. B***347**, 143 (1995); S. Alekhin et al., *Phys. Rev.***D81**, 014032 (2010); S. Alekhin, S. Moch. arXiv:1107.0469 (2001); S. Alekhin, J. Blümlein, S. Moch, *Phys. Rev. D***86**, 054009 (2012); S. Alekhin et al., *Phys. Rev. D***96**, 014011 (2017); S. Alekhin et al., arXiv:0908.3128 [hep-ph](2009); M. Glück et al., *Phys. Lett. B***664**, 133 (2008); H.L. Lai et al., *Phys. Rev. D***82**, 074024 (2010); A.D. Martin et al., *Eur. Phys. J. C***70**, 51 (2010); S. Alekhin and S. Moch, *Phys. Lett. B***699**, 345 (2011).
6. S. Forte et al., *Nucl. Phys. B***834**, 116 (2010); R.D. Ball et al. [NNPDF Collaboration], *Nucl. Phys. B***849**, 296 (2011); R.D. Ball et al. [NNPDF Collaboration], *Nucl. Phys. B***855**, 153 (2012); R.D. Ball et al. arXiv:1710.05935 (2017).
7. R.Thorne, *Phys.Rev.D***73**, 054019 (2006); R.Thorne, *Phys.Rev.D***86**, 074017 (2012).
8. M.Klein, arXiv :1802.04317 [hep-ph] (2018); M.Klein, *Ann.Phys.***528**, 138(2016); N.Armeisto et al., *Phys.Rev.D***100**, 074022(2019).
9. J.Abelaira Fernandez et al., [LHeC Collaboration], *J.Phys.G***39**, 075001(2012); P.Agostini et al., [LHeC Collaboration and FCC-he Study Group], CERN-ACC-Note -2020-002, arXiv:2007.14491 [hep-ex](2020).
10. A. Abada et al., [FCC Collaboration], *Eur.Phys.J.C***79**, 474(2019).
11. B.W.Harris and J.Smith, *Phys.Rev.D***57**, 2806 (1998).
12. LHeC data, <http://hep.ph.liv.ac.uk/~mklein/lhecddata/>.
13. Heavy Q data, <http://hep.ph.liv.ac.uk/~mklein/heavydata/>.
14. R. Abdul khalek, et al., *SciPost Phys.***7**, 051 (2019).
15. S. Alekhin, J.Blümlein and S. Moch, arXiv:2006.07032 [hep-ph] (2020).
16. Wu-Ki Tung, S.Kretzer and C.Schmidt, *J.Phys.G***28**, 983(2002).
17. U.Baur and J.J.Van Der Bij, *Nucl.Phys.B***304**, 451(1988); A. Y. Illarionov, B. A. Kniehl and A. V. Kotikov, *Phys.Lett. B***663**, 66 (2008); S. Catani and F. Hautmann, *Nucl. Phys. B***427**, 475(1994); S. Riemersma, J. Smith and W. L. van Neerven, *Phys. Lett. B***347**, 143(1995); F. P. Wißbrock, DESY-THESIS-2015-040 (2015); B.W. Harris and J. Smith, *Nucl.Phys. B***452**, 109(1995).
18. I.P.Ivanov and N.N.Nikolaev, arXiv:hep-ph/0004206 (2000); J.Lan et al., *Phys.Rev. D***102**, 014020 (2020); J.Lan et al., *Phys.Rev. D***101**, 034024 (2020); C.Mondal, *Eur.Phys.J.C***76**, 74(2016).
19. A.Donnachie and P.V.Landshoff, *Z.Phys.C***61**, 139(1994); *Phys.Lett.B***518**, 63(2001); *Phys.Lett.B***533**, 277(2002); *Phys.Lett.B***470**, 243(1999); *Phys.Lett.B***550**, 160(2002); R.D.Ball and P.V.landshoff, *J.Phys.G***26**, 672(2000); P.V.landshoff, arXiv:hep-ph/0203084 (2002).
20. N.N.Nikolaev and V.R.Zoller, *Phys.Lett. B***509**, 283(2001); A. V. Kotikov, A. V. Lipatov, G. Parente and N. P. Zotov *Eur. Phys.J.C***26**, 51(2002).
21. C.Adloff et al. [H1 Collaboration], *Phys.Lett.B***520**, 183(2001); R.D.Ball et al., *Eur.Phys.J.C***76**, 383(2016); G.R.Boroun, *Eur.Phys.J.Plus***135**, 68(2020); B.Rezaei and G.R.Boroun, *Eur.Phys.J.A***55**, 66(2019).
22. J.Bartels et al., *Acta.Phys.Polon.B***33**, 2853(2002); J.Bartels et al., *Phys.Rev.D***66**, 014001(2002); E.Iancu et al., *Phys.Lett.B***590**, 199(2004); A.M.Stasto et al., *Phys.Rev.Lett.***86**, 596 (2001).
23. J.Lan et al., arXiv [nucl-th]:1911.11676 (2019); N.N.Nikolaev and V.R.Zoller, *Phys.Atom.Nucl***73**, 672(2010); N.N.Nikolaev, J.Speth and V.R.Zoller, *Phys.Lett.B***473**, 157(2000); R.Fiore, N.N.Nikolaev and V.R.Zoller, *JETP Lett***90**, 319(2009); A. Y. Illarionov and A. V. Kotikov, *Phys.Atom.Nucl.***75**, 1234 (2012); N.Ya.Ivanov, and B.A.Kniehl, *Eur.Phys.J.C***59**, 647(2009); N.Ya.Ivanov, *Nucl.Phys.B***814**, 142(2009); J.Blümlein, et.al., *Nucl.Phys.B***755**, 272(2006); A.Kotikov, arXiv:1212.3733 [hep-ph] (2012).
24. G.R.Boroun and B.Rezaei, *Int.J.Mod.Phys.E***24**, 1550063(2015); G.R.Boroun and B.Rezaei, *Nucl.Phys.A***929**, 119(2014); G.R.Boroun, *Nucl.Phys.B***884**, 684(2014); G.R.Boroun and B.Rezaei, *EPL***100**, 41001(2012); G.R.Boroun and B.Rezaei, *J.Exp.Theor.Phys.***115**, 427(2012); G.R.Boroun and B.Rezaei, *Nucl.Phys.B***857**, 143(2012).
25. H.Sun, POS(DIS2018)186; H.Sun, arXiv [hep-ph]:1710.06260(2017); Z.Zhang, arXiv[hep-ex]: 1511.05399 (2015).
26. Ch. Schwanenberger, LHeC worksop, CERN/Chavannes-de-Bogis (2015); Ch. Schwanenberger, POS(DIS2017)464; A.O.Bouzas and F.Larios, *Journal of Physics: Conference Series***651**, 012004(2015).
27. G.R.Boroun, *Phys.Lett.B***744**, 142(2015); G.R.Boroun, *Phys.Lett.B***741**, 197(2015); G.R.Boroun,

- Chin.Phys.C**414**, 013104(2017); G.R.Boroun, PEPAN Lett.**15**, 387(2018); G.R.Boroun , B.Rezaei and S.Heidari, Int.J.Mod.Phys.A**32**, 1750197(2017); B.Rezaei and G.R.Boroun, EPL**130**, 51002(2020); H.Khanpour, Nucl.Phys.B**958**, 115141(2020).
28. A.O.Bouzas and F.Larios, Phys.Rev.D**88**, 094007(2013).
29. V.P.Goncalves and M.V.T.Machado, Phys.Rev.Lett.**91**, 202002(2003); B.Rezaei and G.R.Boroun, Phys.Rev.C**101**, 045202(2020); G.R.Boroun and B.Rezaei, Nucl.Phys.A**990**, 244(2019).
30. Amanda Cooper-Sarkar, arXiv: 1310.0662 [hep-ph](2013); Stanley J.Brodsky, arXiv: 1106.5820 [hep-ph](2011).
31. F.Demartin et al., Phys.Rev.D**82**, 014002(2010).

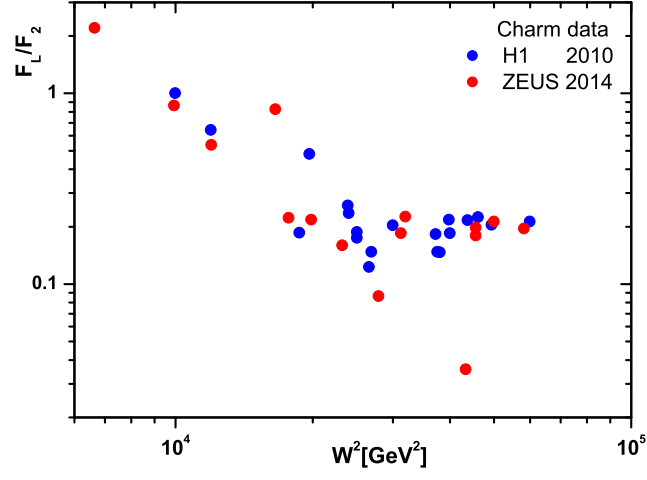


FIG. 1: The ratio of charm structure functions, with respect to HERA data (H1 2010 [1] and ZEUS 2014 [2]), shown as a function of W^2 values.

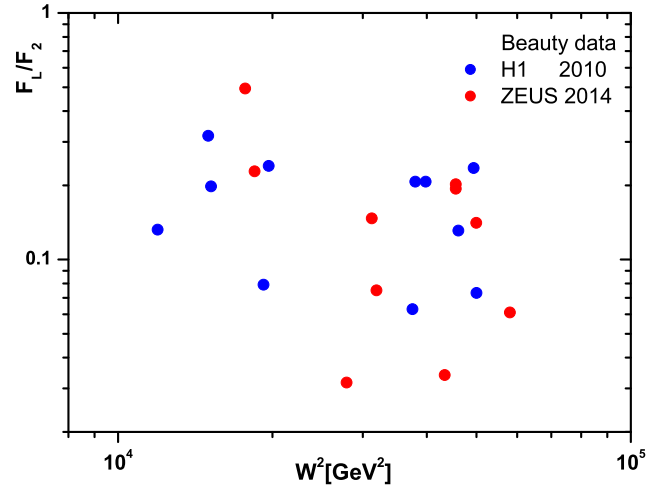


FIG. 2: The ratio of beauty structure functions, with respect to HERA data (H1 2010 [1] and ZEUS 2014 [2]), shown as a function of W^2 values.

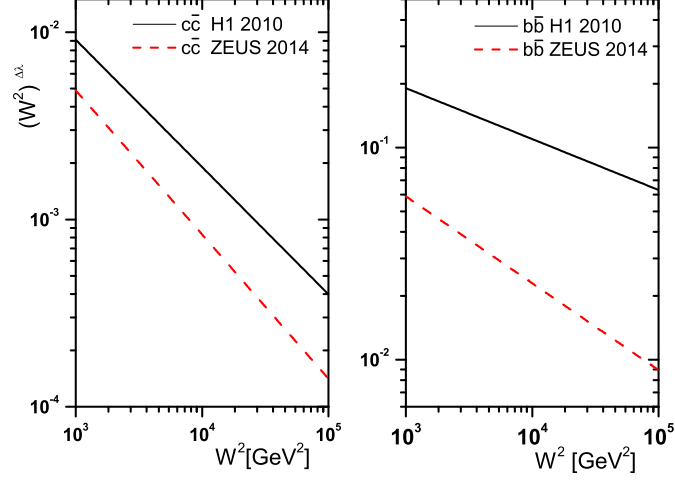


FIG. 3: The behavior of function $(W^2)^{\Delta\lambda}$, for charm and beauty with respect to HERA data (H1 2010 [1] and ZEUS 2014 [2]), shown as a function of W^2 values. $\Delta\lambda = \lambda_L - \lambda_2$ obtained from a linear fit to the structure functions into the invariant center-of- mass energy.

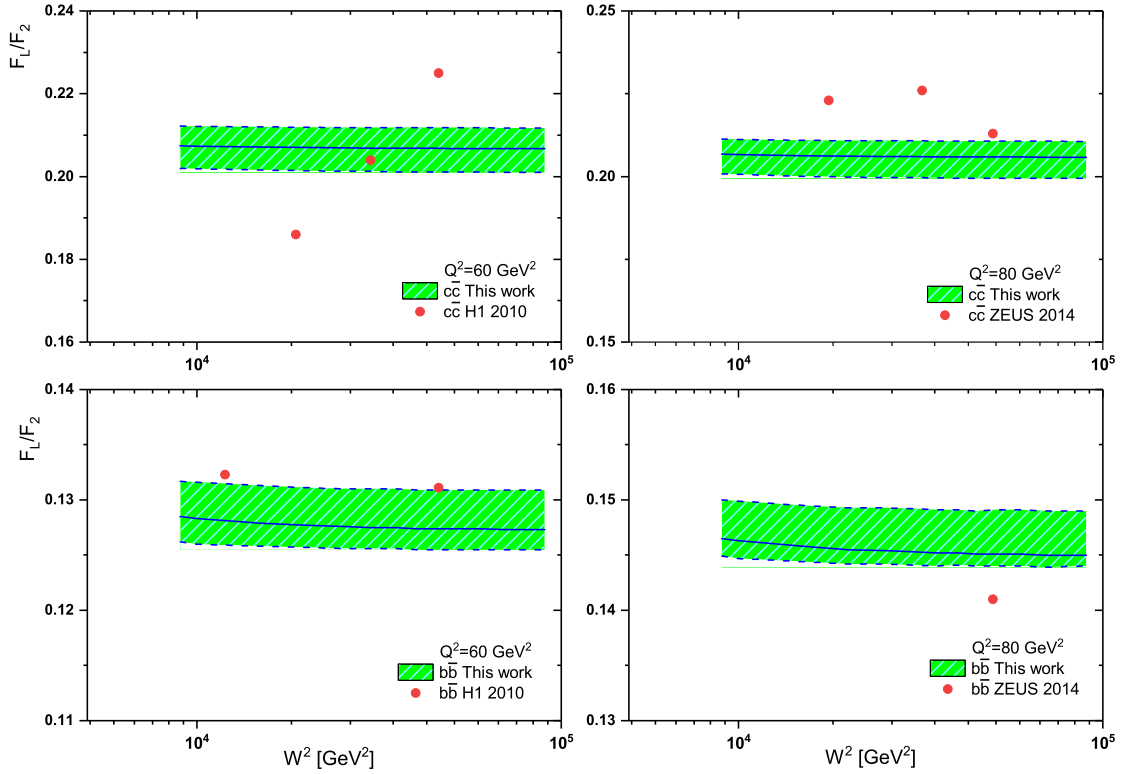


FIG. 4: The obtained $F_L^{Q\bar{Q}}/F_2^{Q\bar{Q}}$ for charm and beauty pair production shown as a function of W^2 for $Q^2 = 60$ and 80 GeV^2 . The error bands show the mass error and the gluon exponent error added in prediction. The combined of HERA data [1,2] are also shown.

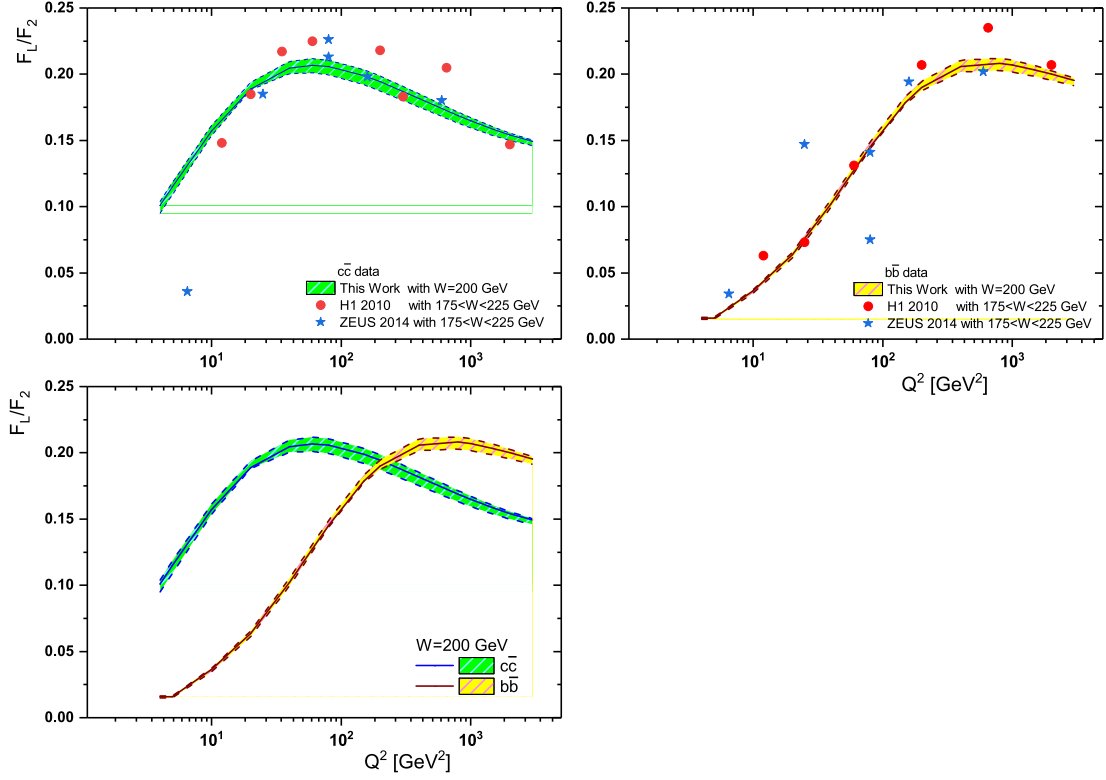


FIG. 5: The ratio $F_L^{Q\bar{Q}}/F_2^{Q\bar{Q}}$ for charm and beauty pair production shown as a function of Q^2 for fixed W^2 value. The error bands show the mass error and the gluon exponent error added in prediction. Our results for charm and beauty are shown in $W = 200$ GeV and compared with H1 2010 [1] and ZEUS 2014 [2] data in $175 < W < 225$ GeV.

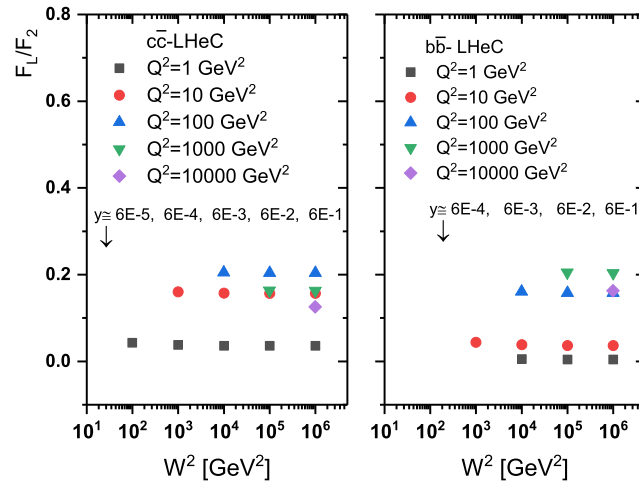


FIG. 6: Theoretical predictions for the ratio of charm and beauty structure functions at $\sqrt{s}=1.3$ TeV (LHeC center-of-mass energy) shown as a function of W^2 for different Q^2 values. The predictions for different inelasticity y values are also shown.

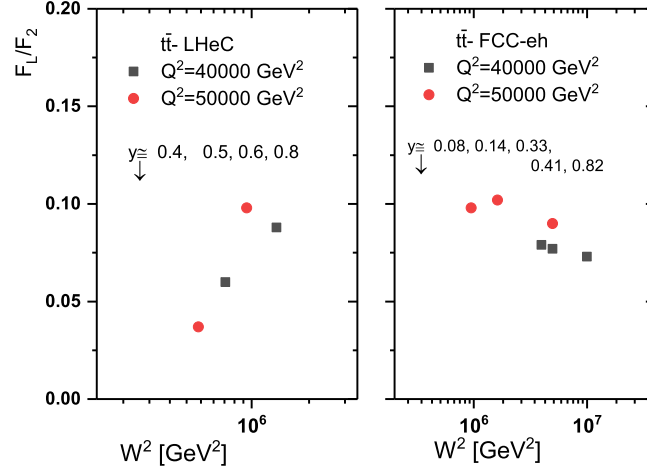


FIG. 7: Theoretical predictions for the ratio of top structure functions at $\sqrt{s}=1.3$ TeV (LHeC center-of-mass energy) and at $\sqrt{s}=3.5$ TeV (FCC-eh center-of-mass energy) shown as a function of W^2 for $Q^2 = 40000$ and 50000 GeV^2 . The predictions for different inelasticity y values are also shown.

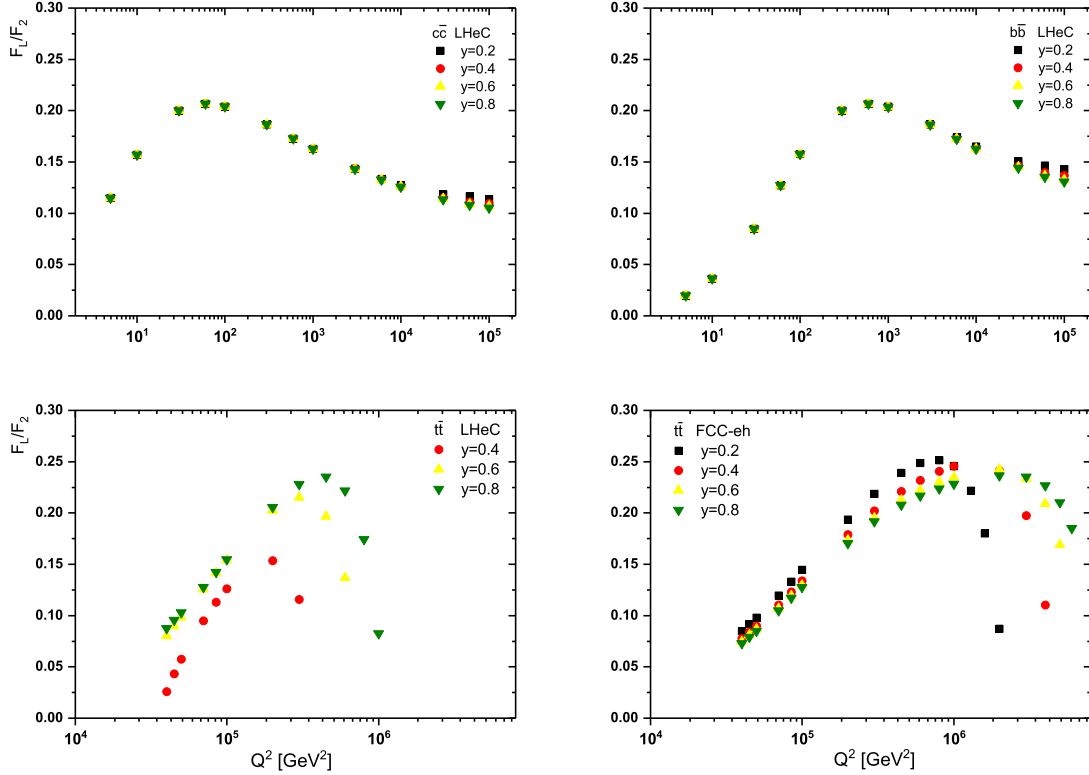


FIG. 8: Theoretical predictions for the ratio of charm and beauty structure functions at LHeC center-of-mass energy and also the ratio of top structure functions at LHeC and FCC-eh center-of-mass energies shown as a function of Q^2 for $y = 0.2, 0.4, 0.6$ and 0.8 .

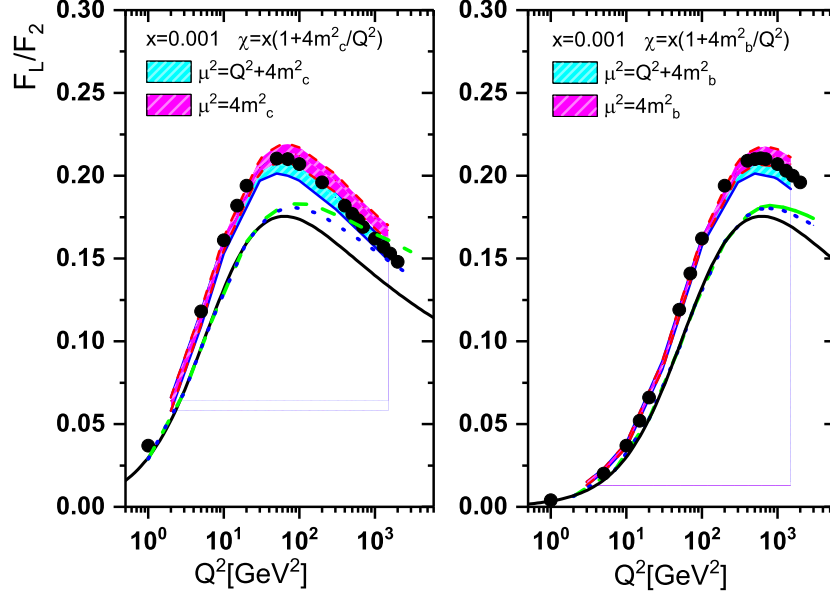


FIG. 9: Comparison of F_L/F_2 calculations for charm and beauty vs. Q^2 with two different choices of μ . These results compared with LO (solid lines) and NLO (dash lines by $\mu = \sqrt{4m^2 + Q^2}$ and dot lines by $\mu = 2m$) quantities from Ref.[17](A. Y. Illarionov, B. A. Kniehl and A. V. Kotikov, Phys.Lett. B **663**, 66(2008)) and also with results Ref.[23](N.Ya.Ivanov, and B.A.Kniehl, Eur.Phys.J.C**59**, 647(2009))(black points) at $x = 0.001$.